Measuring evaporation across canopy phenophases of a natural forest: Miombo forest, Southern Africa.

***H. Zimba[1,2], A.M.J. Coenders-Gerrits[1], K. Banda[3], B. Schilperoort[1], I. Nyambe[3], N.C. van de Giesen[1], H. H. G. Savenije[1].**

[1] Delft University of Technology, Water Resources Section, Building 23 (Faculty of Civil Engineering and Geosciences) 2628 CN Delft, P.O Box 5048 2600 GA Delft, The Netherlands.

[2] Ministry of Agriculture, Department of Agriculture, P.O Box 50595, Mulungushi House, Independence Avenue, Lusaka, Zambia.

[3] University of Zambia, Integrated Water Resources Management Centre, Department of Geology, School of Mines, Great East Road Campus, Lusaka, Zambia.

*Correspondence: h.m.zimba@tudelft.nl

Abstract

Atmospheric water demand drives forest evaporation controlled by the plant physiological properties within available moisture storage thresholds. The pattern and magnitude of African Miombo Forest transpiration across dry season canopy phenophases are unknown. This is because estimating forest evaporation in African ecosystems continues to be a challenge as flux observation towers are scant, if not completely lacking in most ecosystems like the Miombo Forest, one of Africa's largest woodland formations. Moreover, in the Miombo Forest, satellite data-based evaporation products (i.e., GLEAM, MOD16, SSEBop and WaPOR) show significant discrepancies in both pattern and ~~amounts~~ of evaporation especially during the dry season canopy phenophases. Despite the main limitations with estimation of forest evaporation, the development and application of the distributed temperature sensing (DTS) system is providing deepened insights and improved accuracy in forest energy partitioning for evaporation assessment. In this study the Bowen ratio distributed temperature sensing (BR-DTS) approach ~~is~~ used to partition available energy and estimate evaporation across three Miombo Forest canopy phenophases covering the entire 2021 dry season and early rain season. Furthermore, four satellite evaporation products are compared to the field observations. Results show that evaporation appears to follow the net radiation and air temperature pattern with the lowest values observed ~~during the most~~ net radiation and air temperature depressed ~~periods~~ and highest ~~values~~ during the peak net radiation and air temperature. Evaporation continues to rise even during the driest period in the dormant leaf phenophase when canopy cover is ~~said to be~~ at its minimum. This possibly facilitated by the retention of about 70 percent canopy cover during the dry season which transpires within the adapted thresholds constrained by physiological properties of each Miombo Forest species with access to ground water and vegetative water storage. This goes to show that during the dry season Miombo species may not be as water stressed as imagined. When compared to field observations ~~all~~ four satellite evaporation products underestimate evaporation with only the WaPOR showing a similar pattern of evaporation during the dry season. The differences between field observations and satellite-based evaporation products can be attributed to the model structure, processes as well as inputs.

1.0 Introduction

Global terrestrial evaporation is about 60 percent of the total incoming precipitation (Miralles *et al*., 2011; Van Der Ent *et al*., 2014). A large portion, about 78 percent, of this terrestrial evaporation flux is over Africa, Asia and South America (Miralles *et al*., 2011). In Africa, across the vast spectrum of ecosystems, there is a general paucity of evaporation flux observation towers. As a consequence, several satellite evaporation products (e.g., GLEAM, MODIS, SSEBop) are, in most cases, used without validation with field observations from the African ecosystems. In the face of climate change accurate information on evaporation dynamics in major ecosystems, like the Miombo Forest in southern Africa, with significant influence on basin hydrology, is important in the management of scarce water resources. Some studies have been done to validate satellite evaporation products in Africa (e.g.., Blatchford *et al*., 2020; Dile *et al*., 2020; Weerasinghe *et al*., 2020; Ramoelo *et al*., 2014). However, none used field observations based on the Miombo Forest evaporation. In southern Africa, the Miombo Forest is the largest dry forest formation (Frost, 1996) and the characteristic vegetation cover for many river basins including

the Zambezi Basin. The Miombo ecosystem is different from other ecosystems in Africa with unique plant-water interactions (Tian *et al*., 2018; Vinya *et al*., 2018) entailing moisture feedback incomparable to other ecosystems. The typical characteristic of the Miombo species leaf phenology is that they shed off leaves (leaf fall) and also grow new leaves (leaf flush) during what is normally termed ~~as~~ the transition period in the dry season (May – October). Depending on the ~~amounts of~~ rainfall received in the preceding rain season the leaf fall and leaf flush processes may start early (i.e., in case of low rainfall received) or late (in case of high rainfall received) and may ~~go up to~~ November (i.e., in the case of high rainfall received) (Frost, 1996; White, 1984). These typical phenophases require to study the evaporation process in more detail to better assess the limited water resources. Yet, estimating evaporation over natural vegetation like the Miombo Woodland in Southern Africa remains a challenge.

The available accepted approaches such as the eddy covariance (EC) system (Foken *et al*, 2012), lysimeters (Sutanto *et al*, 2012; Teuling ,2018), conventional Bowen ratio (Bowen, 1926) all have limitations. For instance, EC-systems have energy balance closure constraints that affect the measured energy fluxes(Foken, 2008). The two vertical sensor-based Bowen ratio has limitations with having the sensors well aligned which result in each sensor having errors of its own (Angus and Watts, 1984; Spittlehouse and Black, 1980). However, recent advances in distributed temperature sensing system has expanded possibilities for improved accuracy in energy partitioning and the application of the Bowen ratio for evaporation flux assessment in forests (Schilperoort *et al*., 2020; Schilperoort *et al*., 2018; Euser *et al*., 2014). In contrast to the conventional Bowen ratio approach, the Distributed Temperature Sensing Bowen ratio technique (BR-DTS) makes use of several vertical high resolution temperature measurements made with a single fibre optic cable. This eliminates the need for the conventional two individual sensors at different locations and the associated errors with this type of set up. One section of the fibre optic cable measures the air temperature profile, while a second section, covered in a constantly wetted cloth, measures the wet-bulb temperature profile. Through the psychrometric principle, the vapour pressure profile can be derived. With the DTS technique wet and dry bulb temperature measurements can cover the entire vertical profile through a forest stand: above the forest canopy, within the canopy, and under the canopy. This is done simultaneously along a single fibre optic cable, thereby facilitating a deepened understanding of the energy partitioning in a forest (Schilperoort *et al*., 2020; Schilperoort *et al*., 2018; Euser *et al*., 2014). Coenders-Gerrits *et al*.(2020) suggested that the DTS technique offers opportunities to assess forest energy storage components that are not normally captured with conventional approaches. The BR-DTS approach would provide an avenue for enhanced understanding and increased accuracy in the estimation of forest evaporation. This is not withstanding the challenges associated with the BR-DTS approach such as the requirement for sufficient ventilation and constant wetting of the cable. Furthermore, compared to the EC method the BR-DTS approach tend to minimally overestimate diurnal latent heat flux (*LE*) by a mean difference of 18.7 $W.m^{-2}$ (Schilperoort *et al*., 2018).

Additionally, remote sensing based approaches to estimate forest evaporation appeared to show large discrepancies in the Miombo ecosystem (Zimba *et al*., 2022a). Therefore, this study aimed at providing an independent estimation of Miombo Forest evaporation that can be used to validate satellite evaporation products.

In this study field observations ~~are~~ compared with four commonly-used open-source satellite products: GLEAM (Martens *et al*., 2017), MODIS (Mu *et al*., 2011), SSEBop (Savoca *et al*., 2013) and WaPOR (FAO, 2018). These products were selected because they are open source, have comparatively high spatial-temporal resolution and good spatial coverage (i.e., global in the case of GLEAM, MODIS, SSEBop and continental in the case of WaPOR), and are ready to use products with no further processing required. Hence, the focus of this study was on characterising the evaporation in the Miombo Forest using the BR-DTS approach and comparing the field observations with open-source satellite-based evaporation products. Consequently, objectives of this study were to:

1. Measure evaporation in Miombo Forest across canopy/leaf phenophases to help understand the flux pattern in the ecosystem,

2. Compare satellite evaporation products with the field measurements at point scale across Miombo Forest canopy/leaf phenophases.

2.0 Materials and methods

2.1 Study site

The study was centred on a dense Miombo Forest at Nsanzala and Mutinondo conservancy areas (Lat: −12.38, Long: 31.17) in the Mpika District, northern Zambia in southern Africa. Zambia was selected because it is said to have the largest diversity in Miombo Forest species composition (Frost, 1996; White, 1984). The site in

Mpika was chosen because it has a large area of undisturbed Miombo Forest with high species heterogeneity typical of Miombo Forest. It is also located in the largest Miombo Ecosystem component, wetter central Zambezian Miombo (Olson *et al.*, 2001; White, 1984), in the north-western part of the Luangwa Basin (Figure 1).

At the study site, species identification and count within a 250m-by-250m sample plot showed that over 95 percent of the dominant Miombo species is semi-deciduous and include *Brachystegia floribunda, Brachystegia longifolia, Brachystegia boehmii, Brachystegia speciformis, Jubenerdia paninculata, Uapaca kirkiana, Pericopsis angolensis, Bauhinia petersenia* and *Uapaca sansibarica*. These are typical Miombo species, especially the Brachystegia floribunda, found in the wetter Zambezian Miombo Woodland (White, 1984). The typical characteristic of the Miombo species at the site is that they shed off leaves (leaf fall) and also leaf flush during what is normally termed as the transition period in the dry season (May – October). Frost (1996) indicated that, based on the amounts of rainfall received in the preceding rain season, the leaf-fall and leaf flush processes may start early (i.e., in case of low rainfall received) or late (in case of high rainfall received) and may go up to November (i.e., in the case of high rainfall received).

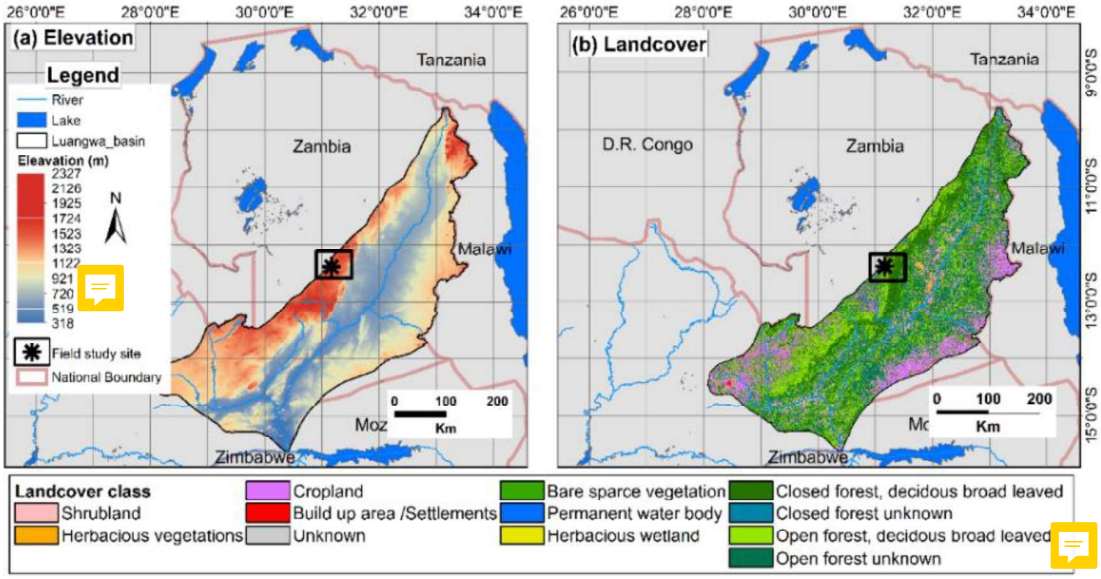

Figure 1. (a) Elevation and land cover (b) characterization in the Luangwa Basin and at the study site in Mpika. The ASTER Digital elevation model was used to depict elevation while the 2019 Copernicus Land cover for Africa was used for land cover characterization.

Mean precipitation at the site is above 1000 mm.year^{-1} and is a result of the movement of the intertropical convergence zone (ITCZ) over Zambia. Mean temperature is about 26 ºC. Rainfall period is between October and April while the dry season is between May and October (Hachigonta and Reason, 2006; Chidumayo, 2001). The forest at the study site is characteristically undisturbed by anthropogenic activities ~~as these~~ are extremely limited due to the site being a conservancy. The major activities in the area are controlled cattle ranching and tourist ~~camping~~. ~~Bush fires are extremely controlled,~~ normally done in August when the Dambos (wetlands) are dry, and ~~is~~ mainly done in the Dambo grassland for livestock grazing purposes.

2.2.0 Approach

This study compared evaporation estimates by the BR-DTS method with the Penman-Monteith reference evaporation (Allen *et al*., 1998) and with four satellite evaporation products at point scale in the Miombo Forest. The observations were done for the period May to December 2021, and facilitated assessment of evaporation during the wet and dry seasons across three different Miombo Woodland canopy phenophases. Characterisation of phenophases (i.e., canopy/leaf phenology calendar) at the study site based on long-term (2009-2017) time series ~~can be seen in~~ Zimba *et al*. (2022a) and Zimba *et al*. (2020). However, for this study the phenophases ~~are~~ based on the 2021 calendar for the period May-December and ~~have been~~ categorised into three groups i.e., Green-down (May-June), Dormant (July-September) and green-up/Mid-green-up (October -December). For easy of comparison with satellite products the green-up phenophase includes the Maturity phenophase which is normally attained around December when the rains begin to stabilize.

2.2.1 Estimating potential evaporation

The Penman-Monteith (PM) equation (i.e., equation 6 in Allen *et al*., 1998) was used to estimate reference evaporation (E_o) from which potential evaporation for the Miombo Forest was calculated using equation 1. All required inputs for the PM equation were obtained at the study site. To obtain potential evaporation for the Miombo Forest the crop coefficient (*Kc*) value of 0.8 was used. The *Kc* value used was obtained from literature (Hunink *et al*., 2015) and was applied in the Miombo Forest in Tanzania. The *Kc* for Mahele region in Tanzania was utilised because it is in the wet Miombo region receiving rainfall of about 1000 mm.year^{-1} with similar seasonality as the study site in Mpika in which rainfall starts late October and ends early May (Hunink *et al*., 2015). Furthermore, despite its vast expanse there is unexpectedly little variation in Miombo Woodland (Chidumayo and Gumbo, 2010). We applied the same *Kc* value for both dry and rainy season.

$$E_{c(PM)} = K_c . E_o \quad (1)$$

2.2.2 Conventional Bowen ratio energy balance method

The Bowen ratio is the ratio of the sensible (H) and latent heat flux (*LE*) of a surface. In simple form the Bowen ratio can be determined by multiplying the psychrometric constant by the ratio of the temperature and vapour pressure gradients as expressed in equation 2.

$$\beta \approx \gamma . \Delta T_a / \Delta e_a \quad (2)$$

Where γ is the pyschrometric constant (kPa.K^{-1}) (equation 3), ΔT_a is the difference in temperature (K) between two heights and Δe_a is the difference in the actual vapor pressure (kPa) between the same two heights. The psychrometric constant is obtained using the relationship between air pressure and ventilation of the psychrometer as given by Allen *et al.* (1998) in equation 3.

$$\gamma = 0.0665 \times 10^3 . P \quad (3)$$

Where, P is the atmospheric air pressure (kPa).

Despite the simplicity of the approach, the energy balance Bowen ratio method needs to meet several conditions in its application ~~if~~ results ~~are~~ to be reliable. For instance, the two levels at which the temperature and vapor pressure ~~measurements are done~~ must be within the boundary layer of the air flow which has adjusted to that particular surface. ~~This requirement entails the field set up must ensure~~ an extensive fetch in the upwind direction for the airflow over the surface. ~~The fetch is suggested to be~~ at least 100 times the maximum height of measurement (Angus and Watts, 1984).

2.2.3 BR-DTS energy balance approach

The BR-DTS method measures air temperature gradients directly and the vapour pressure gradients are estimated via the wet bulb temperatures using equation 4:

$$ea_{Ta} = es_{T_w} - \gamma (T_a - T_w) \quad (4)$$

Where ea_{Ta} is the actual vapour pressure, es_{T_w} is the saturated vapour pressure, γ is the psychrometric constant, T_a and T_w are the dry bulb and wet bulb temperature. Details on this calculation can be found in Schilperoort et al. (2018).

In contrast to the conventional Bowen Ratio Energy Balance, where only the temperature and vapour pressure at two heights are used, the BR-DTS method uses all measuring points between two heights. This is done in order reduce uncertainty from instrument measurement noise. All dry and wet bulb temperatures within this segment are used to determine the gradients according to a natural logarithmic of the height (equations 5 and 6).

$$T_{a_{fit}} = a . \ln(z) + b \quad (5)$$

$$e_{a_{fit}} = c . \ln(z) + d \quad (6)$$

The fitted DTS temperature and actual vapour pressure at 11 m (bottom) and 15.5 m (top) heights above the canopy were used to estimate the Bowen Ratio following equations 7- 9.

$$\beta = \gamma . \frac{\Delta T_{a,\ fit}}{\Delta z} \Big/ \frac{\Delta e_a}{\Delta z} \quad (7)$$

in which;

$$\Delta T_{a.\ fit}/\Delta_Z = T_{a.\ fit}\,(Z=top)\text{-}T_{a.\ fit}(Z=bottom)/(top\ \text{-}bottom)\ +\Gamma\ (z) \quad (8)$$

and

$$\frac{\Delta e_{a.\ fit}}{\Delta_Z} = \frac{e_{a.\ fit}\,(Z=top)\text{-}e_{a.\ fit}(Z=bottom)}{top\ \text{-}\ bottom} \quad (9)$$

Where $\Delta T_{a.\ fit}$ is the difference in air temperature (K) of the fitted curve between the bottom and top of the height range used for the Bowen ratio, $\Delta e_{a.\ fit}$ is the difference in actual vapor pressure (kPa) of the fitted curve over the same height as in temperature, Δ_Z is the difference in height (m) between the two points and Γ is the adiabatic lapse rate. To overcome challenges associated with very small temperature and vapor pressure gradients which could result in errors in the estimation of the Bowen ratio the use of lapse rate is advised especially during dry and unsaturated conditions (Schilperoort *et al.*,2018; Barr *et al.*, 1994). In this study the lapse rate was applied throughout the study period following Schilperoort et al. (2018). Before fitting the data the raw DTS data was calibrated following the approach by des Tombe *et al.* (2020).

2.2.4 DTS data quality control

The quality control process followed the demonstration by Schilperoort *et al.* (2018) as shown in equations 10 and 11. The correlation coefficient of determination (r^2) values for fitted vapour pressure below 0.2 and Bowen ratio values approaching -1.1 and -0.9 were removed from the data for analysis. The coefficients for dry and wet bulb temperature were not considered because the high uncertainty in temperature is propagated in vapour pressure.

$$\text{Flag 1: } r^2_{ea,\,z} > 0.20, \quad (10)$$

$$\text{Flag 2: } \beta < -1.1 \text{ or } \beta > -0.9. \quad (11)$$

Only diurnal temperature and actual vapour pressure data i.e., between 06AM 06PM were considered.

2.2.5 Actual evaporation estimation

Several studies (i.e., Buttar *et al.*, 2018; Euser *et al.*, 2014; Xing *et al.*, 2008; Spittlehouse and Black, 1980) demonstrated the use of the Bowen ratio in combination with the energy balance to assess the latent heat flux. In combination with other energy terms the Bowen ratio energy balance estimate of evaporation (E_β) can be done using equation 12.

$$E_\beta = (R_n - M - G_s)/L(1+\beta) \quad (12)$$

Where R_n is the net radiation flux (W.m^{-2}), L being the latent heat of vaporization of water (2.45 MJ.kg^{-1}), G_s is the ground heat flux (W.m^{-2}) and the M is the change in energy storage in the system canopy storage (W.m^{-2}). The ground heat flux in this study was estimated from the net radiation at hourly intervals. According to the Food and Agriculture Organisation (FAO) (Allen et al. 1998) the ground heat flux for hourly (G_{hr}) or shorter periods can be estimated from net radiation (R_n) using equation 13 during daylight and equation 14 during night-time periods.

$$G_{hr} = 0.1R_n \quad (13)$$

$$G_{hr} = 0.5R_n \quad (14)$$

In this study M was considered negligible and was thus not included in the estimates. The E_β was estimated at hourly intervals and then summed up into daily and 10-day values.

2.2.6 Satellite product comparison

For comparison with satellite evaporation products, field evaporation estimates were categorized into 10-day (decadal) data sets to be in tandem with the satellite evaporation products temporal scales. The native spatial resolutions (Table 1) of the satellite products were used because these products are mostly applied or used in their native resolution configuration. ~~Sources and characteristics of the satellite-based evaporation products used in this study are summarized in Table~~ All products used ~~are~~ open access and thus readily available. In the context of Africa, ~~especially with the aspect of resource limitations,~~ open access to satellite evaporation products is a significant advantage. Furthermore, in the context of this study, sufficient historical data was available and all

products are continuously being processed which assures, to a large extent, future availability of data for continued monitoring. Except for the WaPOR, which has a continental spatial extent, the rest of the products have a global spatial extent. However, all products adequately covered the extent of the Miombo Woodland which was the focus of this study. The rest of the products were accessed online from different product platforms as indicated in Table 1. Details of the methods for each satellite evaporation product can be found in the specific documents cited in Table 1.

2.2.7 Statistical analysis

Statistical comparison of the satellite evaporation products to field observations was done based on the coefficients of determination (R^2) (equation 15), Root Mean Square Error (RMSE) (Equation 16) and the mean bias error (MBE) (equation 17). These are some of the commonly used statistical techniques for comparing pairs of variables and assessing performance of models with reference to observations (Helsel *et al*., 2020). Three statistical approaches were used to compensate for inherent weaknesses in each method. Use of only one statistical may result in incorrect assessment of model performance. A combination of approaches is recommended (Ritter and Muñoz-Carpenaet, 2013). The coefficient of determination measures the strength of relationship between the observed with the modelled values. The closer to 1 the R^2 value is the stronger the relationship of the variables. The RMSE quantifies the deviation of the predicted values from the observed values. The closer to zero the RMSE value is the better the model prediction(s). The Bias is the measure of the extent to which modelled values deviate from observed values and indicates whether there is under or overestimation. The smaller the Bias value the less the deviation of the predicted values from the observed values (Helsel *et al*., 2020). Negative value indicates model underestimation while a positive value indicates overestimation.

$$R^2 = 1 - \frac{\sum_i (O_i - P_i)^2}{\sum_i (O_i - \bar{O})^2} \quad (15)$$

$$RMSE = \sqrt{\frac{1}{n}\sum_{i=1}^{n}(p_i - o_i)^2} \quad (16)$$

$$MBE = \frac{1}{n}\sum_{i=1}^{n}(p_i - o_i) \quad (17)$$

Where, O_i is the flux tower observed evaporation, $\bar{O}$ is the mean of the observed evaporation, P_i is the modelled evaporation and n is the number of observations.

Table 1. Characteristics of the satellite evaporation products used in this study

Evaporation product	Spatial coverage	Temporal resolution	Spatial resolution	Estimation approach	Source of input data	Reference	Source of data
SSEBop	Global	Decadal	1000 m	P–M equation, ET fractions from T_s estimates	MODIS	(Savoca et al., 2013).	Climate engine
Access: https://clim-engine.appspot.com/climateEngine (Accessed 2020)							
WaPOR v2.	Continental	Decadal	250 m	P–M Equation, calculates E, T and I separately	MODIS		WaPOR Portal
Access: https://wapor.apps.fao.org/home/WAPOR_2/1?theme=L1_AETI_D&dim=DEKAD:%255B2020-08-11%252C2020-08-21)							
GLEAM (v3.6a and v3.6b)	Global	Daily	27000 m	P–T equation, soil stress factor	AMSR-E, LPRM, MSWEP+MSWX	(Martens et al., 2017); (Miralles et al., 2011)	FTP server
Access: https://www.gleam.eu/							
MOD16	Global	8-day	500 m	P–M equation, surface conductance model	MODIS	(Mu et al., 2011)	Global subsets tool: MODIS/VIIRS Land Products
Access: https://modis.ornl.gov/globalsubset/							

290 300 310

2.2.8 Flux observation tower setup

Temperature was measured using a single 3 mm 1km long white jacket duplex single tube fibre optic cable connected to the DTS machine. The cable had the ends spliced together to loop the signal back making a double ended configuration. Double ended configuration is explained in (van de Giesen *et al*., 2012). The DTS machine used is the Silixa XT-DTS (Silixa Ltd, 2016) with sensing capabilities as shown in ~~Table A1 in appendices.~~ A calibration bath was set up in which 10 m of the fibre cable from the DTS was placed in water together with 2 x2 PT-100 probes for the entire period of the measurements. The DTS was set to take temperature measurements at a 5 minutes interval. The fibre optic cable was firmly secured on a 17.25 m vertical tower (illustrated in Figure 2 and Figure 3) following the techniques demonstrated by Euser *et al*. (2014) and Schilperoort *et al*. (2018).

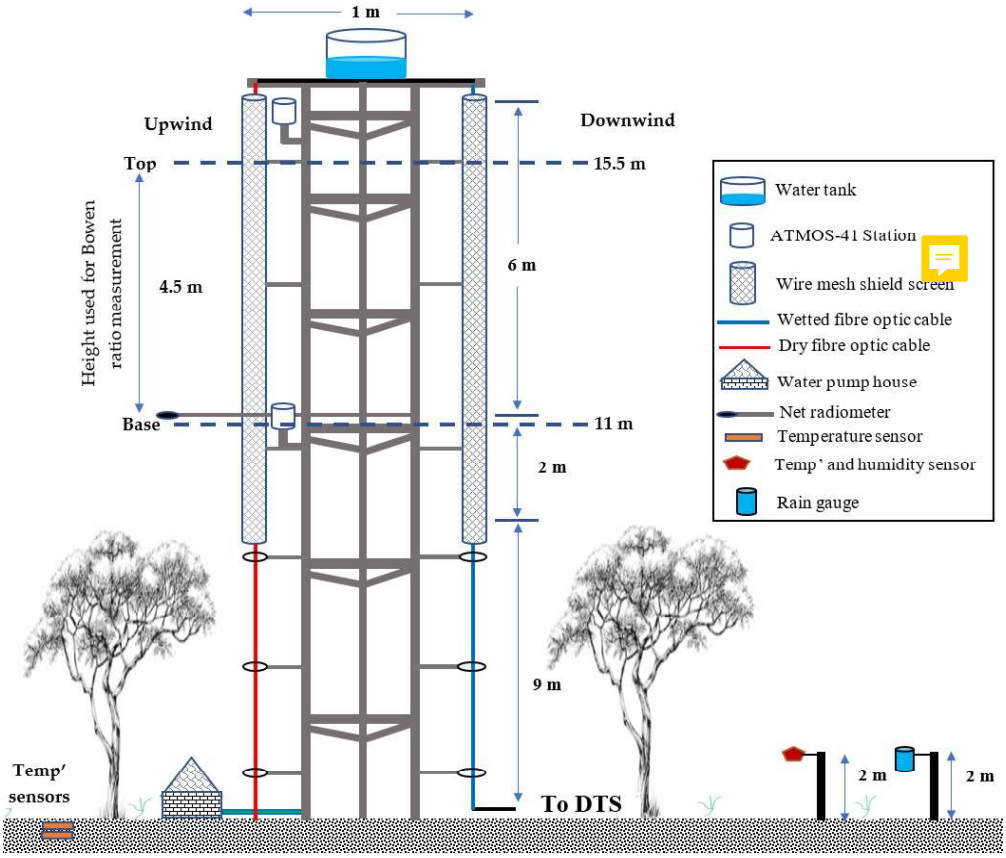

Figure 2. Schematic drawing (not to scale) of the field set-up of the observation tower at the study site in Mpika, Zambia.

Figure 3. Installing the wet (left) and dry (right) fibre optic cable on the observation tower at Mpika site, Zambia. Under canopy view without screens.

One section of the fibre cable (blue line in Figure 2) from the DTS machine was wrapped in cotton cloth (Figure 3 left) starting at the base up to the top of the tower and was always kept wet for estimation of what is known as wet bulb temperature. Separated by a 1 m gap the other section of the fibre cable (red cable in Figure 2) was not wrapped (Figure 3 right) in a cotton cloth and was designated to measure the air temperature. The cloth on the designated wet cable was kept constantly wet by the water that was pumped to the 65-litre tank placed at the top of the tower. The water flow from the water tank to the fibre cable was regulated (roughly 20 litres per day) to ensure a smooth and constant wetting of the cotton cloth. As recommended by Euser *et al*. (2014) the wet cable was placed on the downwind side while the dry cable was placed on the upwind side of the tower. This was done in order to avoid water from the wetted cotton cloth for the wet cable ~~to~~ splash onto the dry cable and thereby affect the dry bulb temperature measurements. Furthermore, there was a gap of 1 m that also contributed to ensuring that the dry cable was not affected by the water from the wetted cotton cloth. Following the recommendation by Schilperoort *et al*. (2018) both the wet and dry cable were shielded from direct sunlight by 8-meter long two layered wire mesh screens placed above the canopy (Figure 2).

A portion of data, ~~about~~ 2 m ~~at~~ the top of the tower, was not included in the assessment because it was assumed to influence the wet clothe/wet cable temperature as the water from the tank above the tower was at ~~slightly higher~~ temperature. The 2 m length was ~~observed~~ sufficient length for the temperature of the water from the tank to be uniform with the environment and suitable for measurement of wet bulb temperature. For this study the tower height was 17.25 m and the fetch was more than 1.7 km. The fetch was in an area with more than 20 km of uninterrupted Miombo Woodland with typical sporadic small seasonal wet grasslands (Figure A1 (b) in the appendices). Furthermore, Spittlehouse and Black (1980) showed that greater accuracy in the Bowen ratio measurements could be attained by increasing the separation between and interchanging the psychrometers. In this study we ensured that there was more than 4 metres separation between the two levels at which the temperature and actual vapour pressure were selected above the forest canopy.

To obtain the net radiation (R_n, W.m^{-2}) the NR Lite 2 net radiometer was installed at 3 m above the forest canopy (that is 11 meters from the forest floor) (Figure 2). The net radiation was logged at hourly interval using the Campbell XR10 data logger. The hourly ground heat flux (G_o, W.m^{-2}) was estimated from the net radiation following the recommendation by Allen *et al*. (1998). The soil moisture was obtained using two soil moisture probes placed at 5 cm and 30 cm in the soil sub-surface. The under-canopy air temperature and relative humidity were obtained at 2 m above the ground and logged at 5 minutes interval using ~~the~~ HOBO data logger. Rainfall was measured with a rain gauge and logged at 5 minutes interval using ~~the~~ HOBO data logger as illustrated in Figure 2.

The air temperature and actual vapour pressure to compare with the DTS measurements were obtained using ATMOS-41 all-in-one weather station sensors. The ATMOS-41 sensors meet standards for the World Meteorological organization (WMO). Details on the capabilities of the ATMOS-41 sensors can be found in the manual (Meter Group AG, 2020). Characteristics of selected ATMOS-41 sensors are given in Table A2 in the appendices. Two ATMOS 41 stations were used one was placed 2 m above the forest canopy (which was 11 meters from the forest floor) while the second station was placed 8 meters above the canopy (16.5 meters from the forest floor) (Figure 2). The ATMOS-41 station sensors were logged at 5 minutes interval same as the DTS.

3.0 Results and discussion

3.1 Evaporation flux foot print/Fetch analysis

Analysis of the evaporation flux foot print was ~~done~~ using the wind rose (Figure A1 in the appendices). The wind rose was used to obtain the most frequent and consistent wind direction to help determine which part of the study site was the major influencer of the evaporation flux. The wind was predominantly coming from the eastern direction with wind speed ranging between $2 - 6$ m.s^{-1}. This made it possible to obtain satellite product values in the correct grids/pixels for comparison with BR-DTS evaporation estimates ($E_{a\,(DTS)}$). Using the identified predominant wind direction, the fetch/flux footprint equal to 100 times the height (17.25 m) of the observation tower was designed. Thus, the fetch/flux footprint was designed to cover a 1.725 by 1.725 km area (approximately 2 km by 2 km grid).

3.2 DTS data quality control

The study period comprised 238 days of which 5 days (2 in June, 2 in August and 1 in September) had entire diurnal period with actual vapour pressure fitting R^2 values below 0.2. For the rest of the days the maximum number of hours with R^2 values below 0.2 and/or $\beta < -1.1$ or $\beta > -0.9$ were 4 which is about 23 percent of the ~~daily~~ diurnal data series. The Bowen ratio values corresponding to diurnal vapour pressure fitting R^2 values below 0.2 were removed and gaps filled using linear regression method based on the diurnal Bowen ratio relationship with diurnal DTS air temperature and net radiation. As a result of poor wetting of the fibre cable one day in September (25th September) and one day in October (30th) were also assessed using regression filled Bowen ratio data. Due

to DTS machine power supply challenges six days in December (26th to 31st) were not available for analysis. Consequently, overall, about 97 percent of the fitted diurnal actual vapour pressure and the Bowen ratio passed the quality test for use in the study. Figure 4 shows the comparison of DTS estimates ~~of~~ air temp[illegible]ure (a, b) and actual vapour pressure (c, d) estimates with the reference ATMOS-41 sensors at the 11 m and 16.[illegible]s above the forest canopy on the tower. Installing ATMOS-41 weather stations above the forest canopy exposed the temperature sensors to direct sunl[illegible]early morning and late afternoon. Consequently, at both 11 m and 16.5 m height direct sun light interaction [illegible] the temperature sensor under the ATMOS-41 influenced the temperature measurements. This resulted in deviations in ATMOS-41 air temperature for the two periods. The relatively warm water from the tank flowing down the cable did not always reach the wet bulb temperature at the 16.5 m height, consequently, the actual vapour pressure was overestimated by the DTS measurements. This probably explains the relatively lower correlation (R^2 = 0.79) of the DTS actual vapour pressure measurements in comparison with the ATMOS-41 measurements at 16.5 m. However, DTS and ATM[illegible]-41 air temperature and actual vapour pressure measurements showed good agreement at 11 m with R^2 = 0.98 [illegible]0.86 respectively (Figure 4 a, c). Overall, DTS measurements and reference estimates by the ATMOS-41 showed good agreement, sufficient for this study, at both heights above the forest canopy.

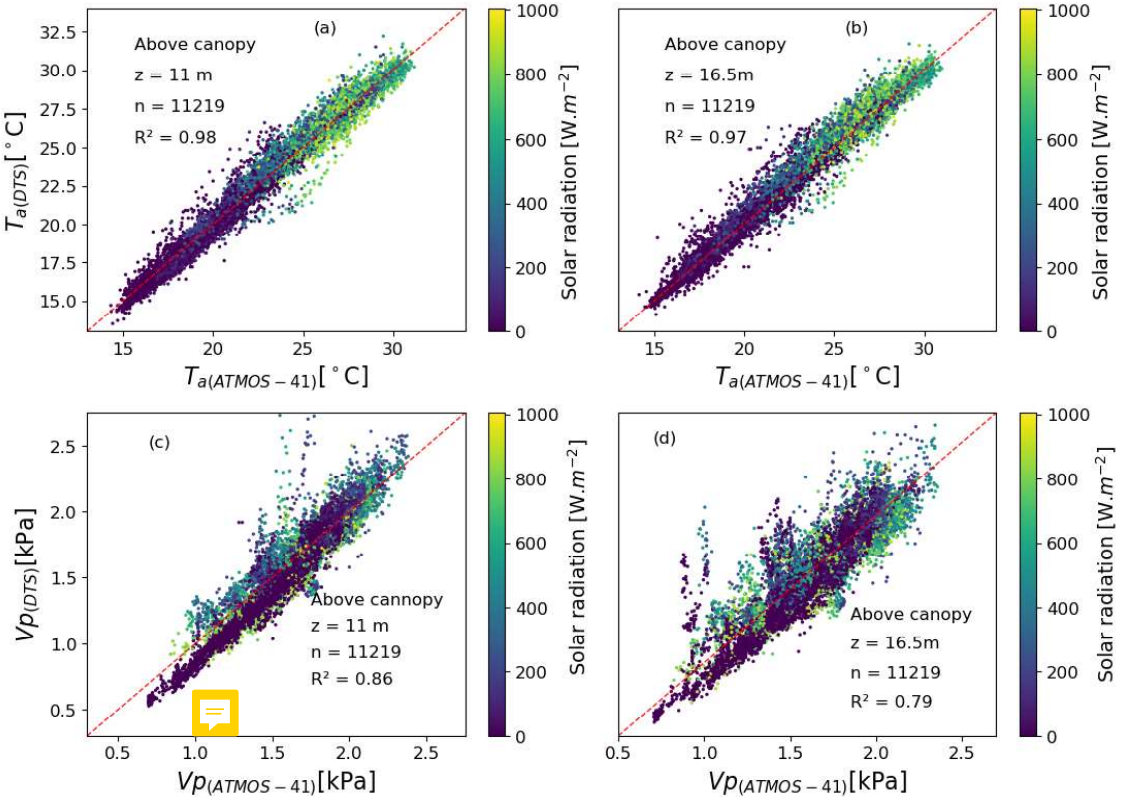

Figure 4. Comparison of DTS temperature ($T_{a\,(DTS)}$) and actual vapour (vp_{DTS}) measurements with the ATMOS-41 ($T_{a(ATMOS-41)}$ and $vp_{ATMOS-41}$) measurements at 11 m and 16.5 m above the forest canopy.

3.3 Meteorological conditions

~~Figure 5 shows the meteorologic[illegible]nditions at the study site for the period May to December 2021~~. The wind direction was mainly easterly and [illegible]stantly oscillated between the North-East and South-East direction (approx. 50 – 110 degrees) (Figure A1 in the [illegible]endices). Wind speed (u) ranged between 0.7 - 8 m.s^{-1} with relatively higher ~~speed~~ observed in the dry season between July and September during the dormant phenophase. Minimum and maximum net radiation (R_N) ~~is~~ observed during the dry season[illegible]d wet season respectively. The drop in air temperature (T_a) and relative humidity (RH) coincides with reduced[illegible] moisture (SM) in the dormant phenophase in dry season (Figure 5). T_a ranged between 7 [illegible]° C. Relative humidity co-varied with T_a and P. Using the Bowen ratio (BRDTS) available energy ~~is~~ partiti[illegible] into sensible (H) and latent heat (LE) fluxes[illegible] H and LE co-varies with ~~latent heat~~ predominantly exceeding ~~sensible heat~~ across phenophases. On days with precipitation (P) the H and LE appeared to be of similar magnitude.

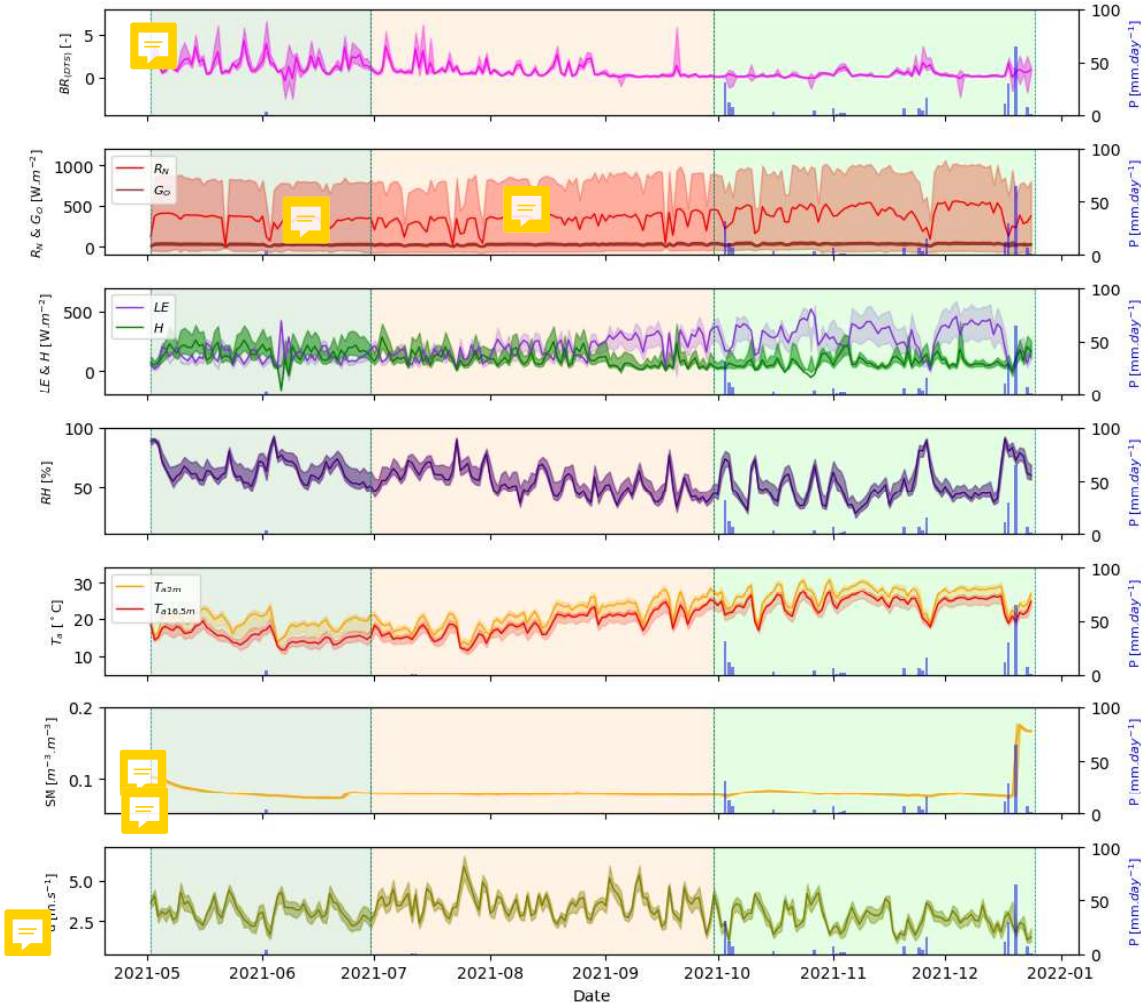

Figure 5. Daily meteorological conditions at the Mpika study site in the Luangwa Basin for the period May 2021 – December 2021. Shaded area May-June is the canopy Green-down phenophase, July-September is the dormant phenophase and October-December is the Green-up phenophase. Shaded area for variables is the standard deviation.

3.40 Canopy phenophase based Bowen ratio and evaporation pattern

~~Figure 6 shows phenophase based average hourly estimates of wind direction, wind speed, net radiation, Bowen ratio and evaporation for t reen-down (i.e., May-June), dormant (i.e., July-September) and green-up (i.e., October - December) phenophases.~~ During the green-down phenophase the Bowen ratio ~~is~~ highest while air temperature ~~is~~ lowest in a relatively lower net radiation and vapour pressure environment. During the dormant and green-up phenophases the Bowen ratio is lowest while the temperature is highest in relatively higher net radiation and lower relative humidity conditions (Figures 5 and 6). The green-down phenophase (i.e., May-June) ~~is the most~~ air temperature and net radiation ~~depressed period~~ (Figures 5 and 6) and exhibits highest mean diurnal Bowen ratio (BR) (i.e., diurnal mean BR ≈ 2.0) indicative of the energy being largely expended as sensible heat compared to the dormant (i.e., diurnal mean BR ≈ 0.35) and green-up (i.e., diurnal mean BR ≈ 0.25) phenophases with raised air temperature and net radiation when the energy ~~is~~ mainly expended as latent heat (i.e., diurnal mean BR < 0.5) (Figures 5 and 6). There is alternating energy partitio g across the canopy phenophases as can be seen through the mean Bowen ratio, sensible and latent heat fluxes (Figures 5 and 6). Diurnal energy partitioning interchange across the three phenophases occur round 06 AM and 06PM (Figure 6). The study site is in a warmer Miombo region (Chidumayo and Gumbo, 2010). The observed alternating energy partitioning (i.e., Bowen ratio) pattern is similar to what has been observed in warm ecosystems and climates (i.e., Cho *et al*., 2012) like the Miombo ecosystem. Consequently, diurnal evaporation pattern at the study site is dependent on energy partitioning, increasing with increase in air temperature ~~,~~ net radiation (Figures 5 and 6).

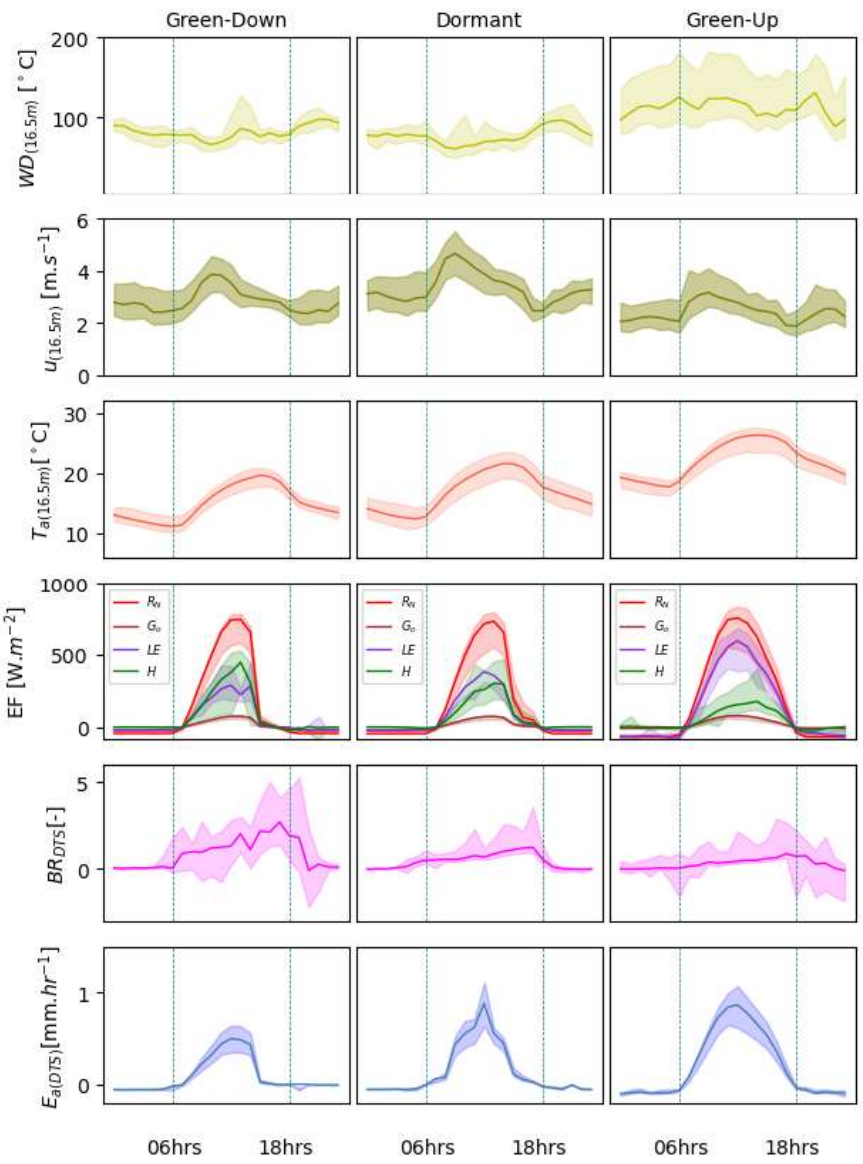

Figure 6. Canopy phenophase based hourly averages of wind direction (WD), wind speed (u), Energy flux (EF) (net radiation (R_N), ground heat flux (G_o), latent heat flux (LE) and sensible heat flux (H)), Bowen ratio (BR_{DTS}) and evaporation ($E_{a\,(DTS)}$). Shaded area is the standard deviation.

3.50 Comparison of daily potential ~~evaporation~~ and actual evaporation

~~Figure 7 shows comparison of estimates of actual evaporation using the BR-DTS ($E_{a\,(DTS)}$) and reference evaporation using the Penman-Monteith (PM) ($E_{c\,(PM)}$) approach~~. $E_{a\,(DTS)}$ was estimated at diurnal (06 AM – 6 PM) hourly interval and then summed up into daily and decadal evaporation. Overall, Miombo Forest potential evaporation $E_{c\,(PM)}$ is higher than $E_{a\,(DTS)}$ by an average of 7 percent per day (Figure 7 a). However, in low temperature conditions (i.e., June – July) on some days the actual evaporation is relatively higher than the potential evaporation (Figure 6a). $E_{a\,(DTS)}$ and $E_{c\,(PM)}$ shows similar pattern across canopy phenophases with strong correlation (R^2 = 0.92) at decadal scale (Figure 7 b). For both $E_{a\,(DTS)}$ and $E_{c\,(PM)}$ significant uncertainties (i.e., standard deviations) where observed in the dormant and green-up phenophases (i.e., August – December) (Figure 7 b, Table A2 in the appendices). This is possibly due to changes in both meteorological conditions and canopy display characteristics (i.e., Figures 5 and 8).

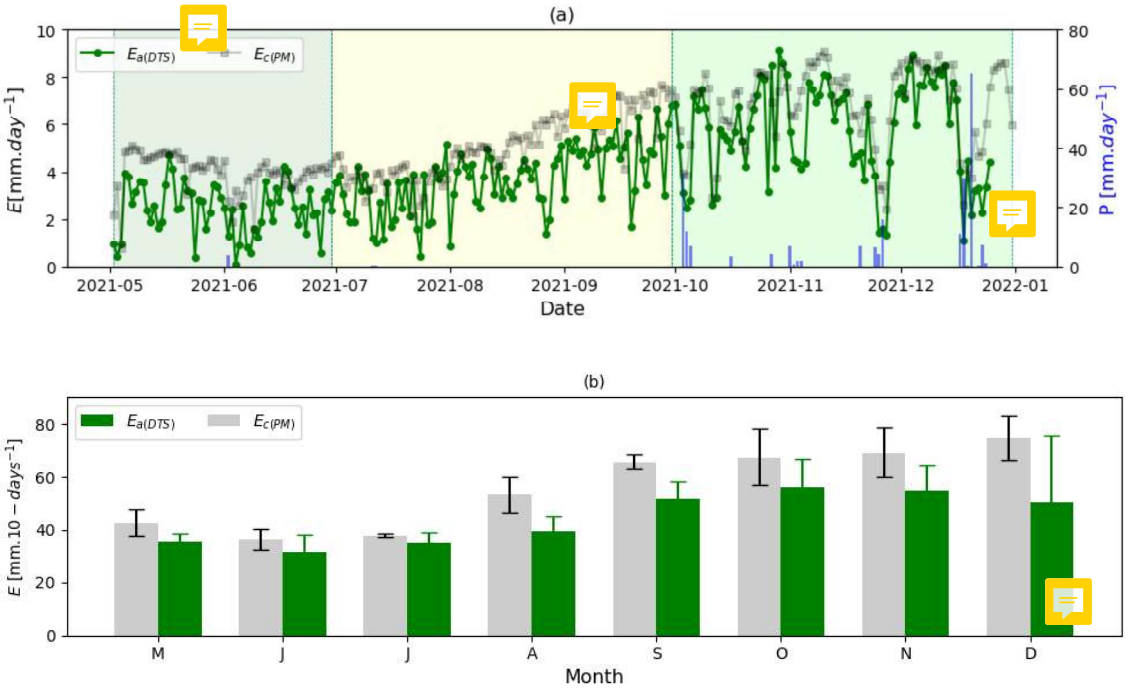

Figure 7. (a) May – December 2021 daily (06AM - 06PM) estimates of evaporation $E_{a\,(DTS)}$ using the BR-DTS and $E_{c\,(PM)}$ using the PM. (b) Comparison of decadal evaporation estimates between $E_{a\,(DTS)}$ estimates and $E_{c\,(PM)}$ (E_c = K_c. Eo). The $E_{a\,(DTS)}$ and $E_{c\,(PM)}$ show good agreement in both dry and rainy seasons as well as across canopy phenophases. Overall, at decadal scale the $E_{c\,(PM)}$ is relatively higher than $E_{a\,(DTS)}$ ~~(b)~~. Shaded area on top are phenophases, May-June is the green-down phenophase, July-September is the Dormant phenophase and October to December is the green-up phenophase.

The BR-DTS approach appear to have correctly captured the moisture feedback of the Miombo Forest across different canopy phenophases. Cumulatively for the period May-December 2021, the $E_{a\,(DTS)}$ estimates are 18 percent less than the potential evaporation for the Miombo Forest as determined with the FAO PM model using meteorological observations at the study site. Actual evaporation, $E_{a\,(DTS)}$, at the study site appears to follow the pattern of available energy (i.e., net radiation, air temperature) and the dynamics in canopy ~~display~~ regimes. For instance, lowest actual evaporation is observed during the most net radiation and air temperature depressed month of June during the green-down phenophase but begins to r with the start in rise in net radiation in July despite the commencement of the leaf fall process in the dormant phenophase. Evaporation continues to rise even during the driest period of the year in the dormant canopy phenophase. In terms of canopy di (i.e., proxied by the normalised difference vegetation index (NDVI)) and vegetation water content (i.e., p by the normalised difference infrared index (NDII)), August/September and not June are the months when the lowest indices values are observed (i.e., Zimba *et al*., 2020). Yet August/September evaporation is higher than that for June. This demonstrates the role of available energy (i.e., as indicated by net radiation) in the Miombo Forest evaporative dynamics. The plausible explanation for the relatively higher evaporation in August and September during the dormant phenophase could be that the leaf fall and leaf colour transitions (i.e., Figure 8) in some Miombo species at a given time, across the three phenophases, is compensated by the leaf flush process in other species thereby striking the dry season 30 percent variation (Frost, 1996) balance in canopy cover display ensuring availability of 70 percent evaporative surfac at increases as the phenophases transition from dormant to green-up. Negative NDII values are indicative of plant water stress conditions (i.e., Sriwongsitanon *et al*., 2015). At the study site long term (2009 - 2018) dormant phenophase lowest mean NDII values were about -0.1 (Zimba *et al*., 2020). This is indicative of peak leaf fall and leaf flush activities (i.e., Figure 8 right). However, it is possible that during the dormant phenophase, the evaporative surface (leaves) is responsive to the increased solar radiation/air temperature (i.e., Figure 5) and the vegetation water demand may correspond to a specific transpiration rate that is within the available vegetative and root zone water storage thresholds (i.e., -0.1 as proxied by the NDII) in agreement with the observations by Tian *et al*. (2018) and Vinya *et al*. (2018). The start in rise in NDII values and the sustained

rise in evaporation in October (green-up phenophase) before commencement of stable rains could be as a result of the increased canopy cover of new leaves with vegetation water demand for transpiration that is, like in the case of the dormant phenophase, within the adapted thresholds of access to ground water and vegetative storage during this period. The marginal drop in November evaporation at the start of the rain season could be attributed to the drop in net radiation and air temperature (Figure 5) influenced by cloud cover and rainfall activity (Figure 7 a) that result in lowered atmospheric water demand as relative humidity increases (Figure 5). The same explanation holds for December although the 6-day DTS data gap (26th – 31st December) contribute to the drop in $E_{a\,(DTS)}$ at decadal scale (Figure 7 b) in comparison to the $E_{c\,(PM)}$.

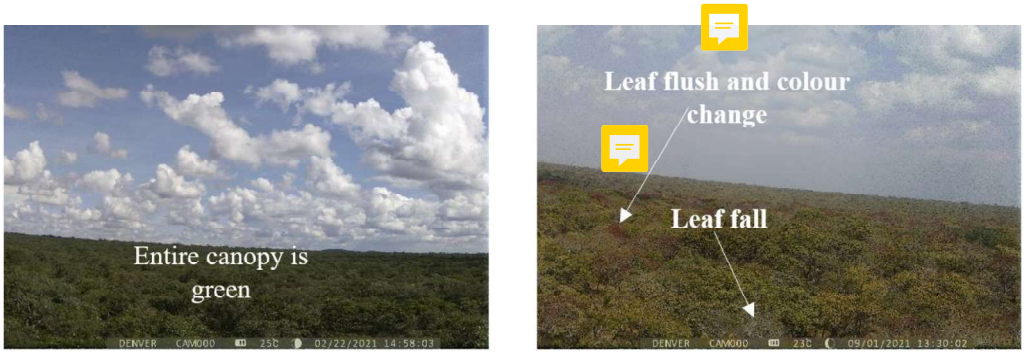

Figure 8. Aerial view of the upwind direction (East direction) above the forest canopy from the flux tower (left) on 22 February 2021 during the peak/maturity phenophase and (right) 01 September 2021 during the dormant phenophase. Differences in canopy leaf colour display at the study site is clearly demonstrated during phenophases.

3.60 Comparison of satellite products with BR-DTS based evaporation

Satellite products GLEAM, MOD16, SSEBop and WaPOR were compared to the $E_{a\,(DTS)}$ and $E_{c\,(PM)}$. Figures 9,10,11 and Tables A3 and A4 in the appendices show the results of the comparison. Of the four satellite products only WaPOR showed a similar pattern to field observations across the three phenophases with a strong overall decal elation coefficient ($r > 0.8$) with both $E_{c\,(PM)}$ and $E_{a\,(DTS)}$ followed by SSEBop ($r = 0.55$ respectively) while MOD16 showed the weakest correlation ($r = 0.37, 0.47$ respectively). To the contrary GLEAM showed negative correlation with observations ($r = -0.49, -0.53$ respectively).

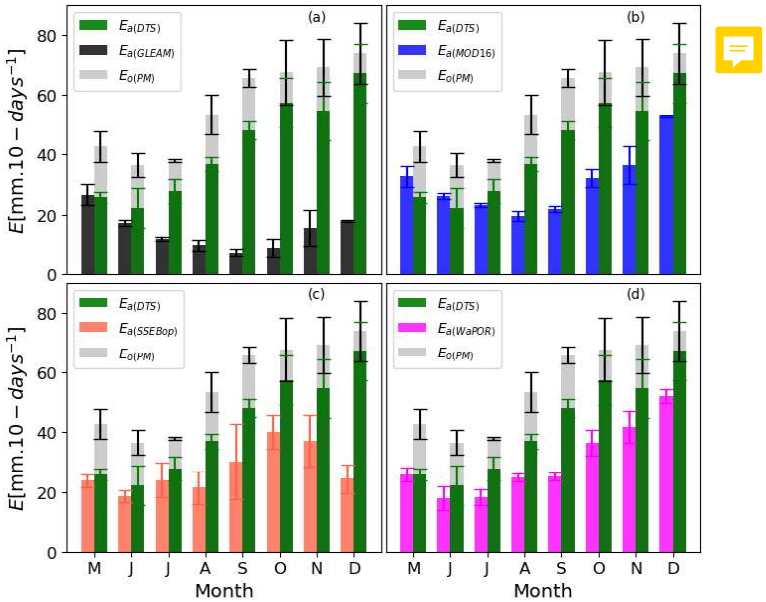

Figure 9. Bar graphs with standard deviation error bars comparing decadal averages of $E_{a\,(DTS)}$ and $E_{c\,(PM)}$ with satellite products at decadal scale. WaPOR shows a similar pattern to both $E_{a\,(DTS)}$ and $E_{c\,(PM)}$ and values closer to the observations compared to GLEAM, MOD16 and SSEBop.

With an exception of MOD16 which showed relatively significant variation in November only (Figure 9 b and Table A3 in the appendices), GLEAM, SSEBop and WaPOR showed significant variations (i.e., relatively larger standard deviations) during the dormant and green-up phenophases (Figure 9 a, c, d and Table A3 in the appendices). ~~Figure 10 shows cumulative $E_{c\ (PM)}$, $E_{a\ (DTS)}$, GLEAM, MOD16, SSEBop and WaPOR evaporation during the three phenophases. Figure 11 shows statistics of the comparison of field observations with satellite products.~~ Overall, the four satellite products underestimate evaporation across the canopy phenophases. Surprisingly, GLEAM appears to strongly underestimate evaporation during the dormant and green-up phenophases. Significant diversion from observed evaporation begins in July at the commencement of the rise in air temperature and net radiation, increased wind speed, commencement of the dormant phenophases (i.e., typified by leaf fall and leaf flush activities). All satellite evaporation products appear to take the same upward trajectory but, with reference to $E_{a\ (DTS)}$ underestimate evaporation. Cumulative $E_{c\ (PM)}$ was about 1270 mm.8-months^{-1}, actual evaporation $E_{a\ (DTS)}$ was estimated at 970 mm.8-months^{-1} which was about 24 percent lower than the potential evaporation. Cumulative GLEAM evaporation was 310 mm.8-month^{-1} about 76 percent lower than potential evaporation and 68 percent lower than actual evaporation $E_{a\ (DTS)}$, MOD16 (682 mm.8-month^{-1}) about 46 percent lower than potential evaporation and 30 percent lower than actual evaporation $E_{a\ (DTS)}$, SSEBop (633 mm.8-month^{-1}) about 50 percent lower than potential evaporation and 35 percent lower than actual evaporation $E_{a\ (DTS)}$ while WaPOR (677 mm.8-month^{-1}) about 47 percent lower than potential evaporation and 30 percent lower than actual evaporation $E_{a\ (DTS)}$ (Figure 10 and Table A3 in the appendices).

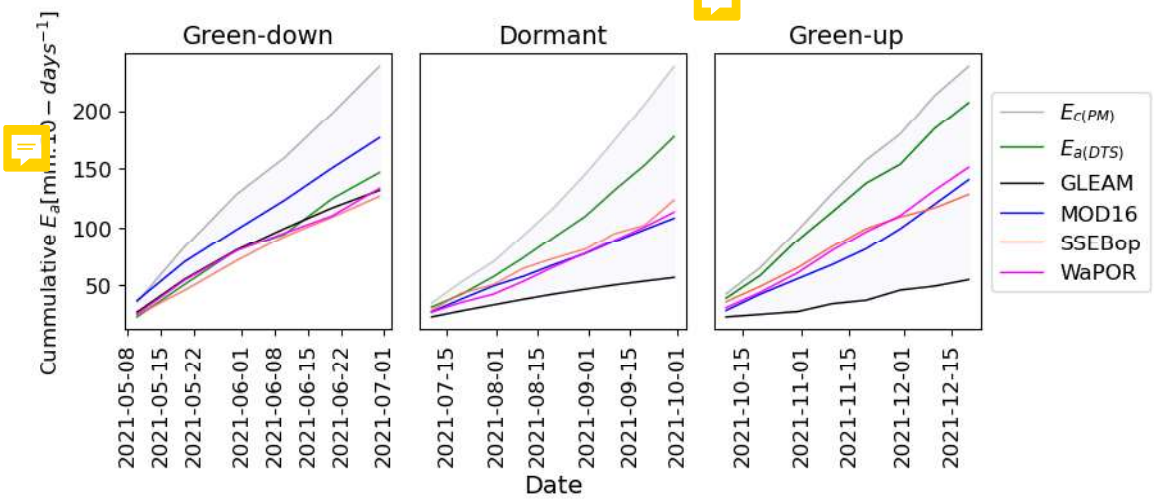

Figure 10. Comparison of cumulative potential evaporation $E_{c\ (PM)}$ and cumulative actual observation $E_{a\ (DTS)}$ with cumulative GLEAM, MOD16, SSEBop and WaPOR for the period May – December 2021 per phenophase. Shaded area is the range between highest and lowest evaporation in each phenophase.

Overall, for the eight-month period, MOD16 and WaPOR shows relatively higher estimates of mean evaporation followed by SSEBop while GLEAM gives the lowest estimates (Table A3 in the appendices). Furthermore, WaPOR showed better positive correlation (r) with field observations across the three phenophases (Figure 11a). GLEAM showed negative correlation during dormant and green-up phenophases as it declined while field observations increased (Figure 11a). The underestimations are mainly associated with the dormant and green-up phenophase (Figure 10) as can be seen from the uncertainty RMSE and MBE values in Figure 11 c, d. MOD16 shows higher bias during the green-down phenophase followed by SSEBop. During the dormant phenophase SSEBop shows relatively lower bias and is followed by WaPOR. In the green-up phenophase WaPOR shows the lowest bias followed by SSEBop. However, compared to other products WaPOR shows minimal MBE during the green-up phenophase while GLEAM shows largest biases during the dormant and green-up phenophases.

Discrepancies in satellite evaporation products behaviour with field observations can be attributed to individual model characteristics. GLEAM has four modules that include the potential evaporation, Rainfall interception, soil and stress modules. The potential evaporation module uses the Priestly and Taylor equation and is driven by observed surface meteorology. The interception module is based on the Gash analytical model and is driven by observed precipitation. The soil module is a multi-layer model driven by observed precipitation and satellite surface soil moisture. The stress module is based on semi-empirical relation to root zone soil moisture and the vegetation optical depth (VOD) (Martens *et al*., 2017).

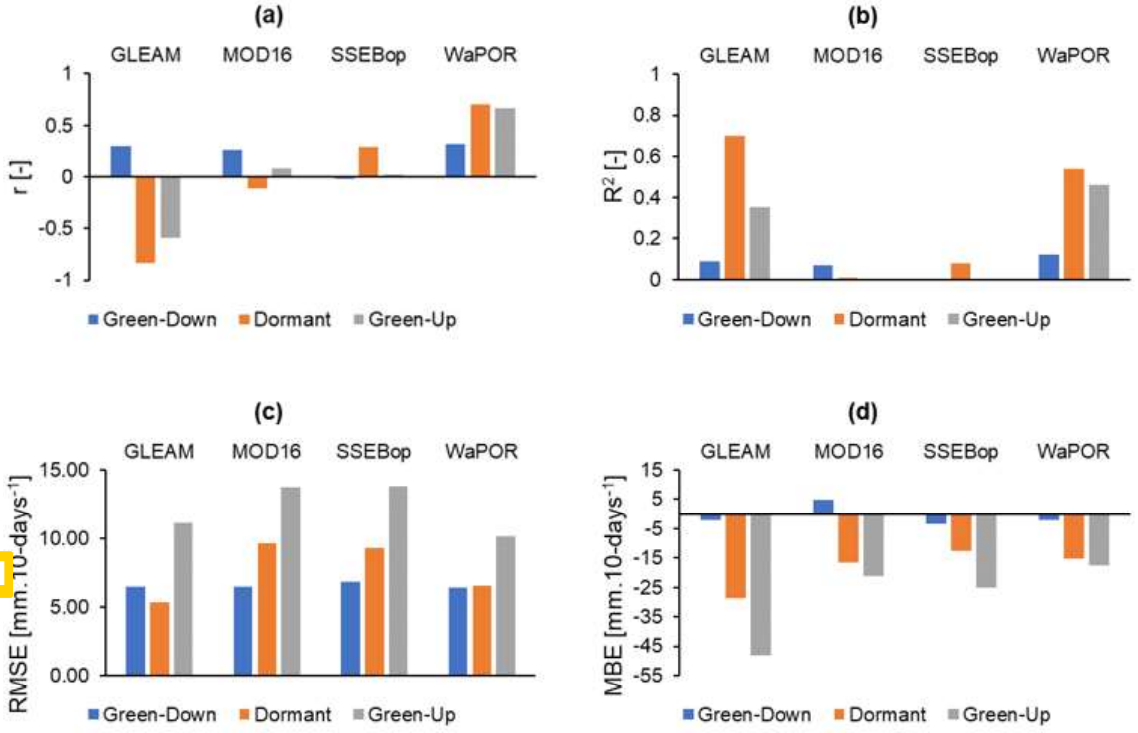

Figure 11: Statistics of the comparison between $E_{a\ (DTS)}$ and satellite evaporation products at decadal scale across canopy phenophases.

GLEAM shows a pattern of continued downward evaporation from the green down phenophase through the dormant phenophase and begins to rise in October during the green up period at the start of the rain season. It shows a similar pattern during the green down and green-up phenophases but different during the dormant phenophase. Probable explanation for this behaviour could be the soil moisture module structure of GLEAM. At the study site, and the Miombo Woodland in general, the green down and dormant phenophases are in the dry season. The soil moisture (i.e., at 30 cm) begins to decline in March at the end of the rain season but stays relatively unchanged throughout the dry season (Figure 5; Zimba *et al.,* 2022b). However, the moisture residue at 30 cm subsurface is relatively higher during the green-down phenophase as compared to the dormant and start of the green-up phenophases. Figures 9, 10 and 11 show GLEAM estimates to be similar with field observations and the other satellite products during the green-down phenophase. This probably shows that GLEAM is sensitive to changes in the precipitation related sub-surface moisture dynamics. The species heterogeneity at the study site, as is common with Miombo Woodland, is high. This means that while some species are shedding off leaves others are experiencing leaf flush. The consequence of this phenomenon is that there is only 30 percent variation in canopy cover throughout the dry season with 70 percent canopy returned at any given time. Therefore, there is sufficient evaporative surface at any given time. The question is whether there is enough water available for evaporation. Studies (e.g., Gumbo *et al*. 2018; Tian *et al*., 2018; Vinya *et al*., 2018**;** Frost, 1996) have shown the Miombo species to have both deep (beyond 5 m depth) and extensive lateral rooting system providing accessing to ground water resources. The plants also have adapted vegetative water storage mechanisms. This possibly explains the pattern of field observations which showed a rise in evaporation during the dormant and green-up phenophases in the dry season. GLEAM soil module only takes into account 250 cm of the sub-surface soil moisture that is linked to observed precipitation. GLEAM drainage algorithm does not take into account horizontal and upward moisture fluxes beyond 250 cm depth. This implies that GLEAM is fully net precipitation based thereby not taking into account the groundwater fluxes that are not related to precipitation. Therefore, GLEAM (v3.6a, v3.6b) is likely not to capture the correct dry season (July- October) Miombo species moisture feedbacks as has been demonstrated in Figures 9 and 10. The ~~start in~~ rise in GLEAM evaporation in October could be attributed to the interception due to rains and sporadic rise in soil moisture in October (Figure 5) and goes to validated GLEAM dependence on net precipitation for actual evaporation assessment. In increased solar radiation and canopy cover (i.e., leaf area index (LAI)) conditions like occurs in October at the study site interception is

likely to be high with a small amount of precipitation and only begins to reduce as precipitation increases. This shows that the GLEAM interception module, possibly aided by the quality of the rainfall product used, i.e., Multi-Source Weighted-Ensemble Precipitation (MSWEP), is responsive in the Miombo Forest. The overall driving factor of GLEAM behaviour, with reference to the field observations of evaporation in this study, might be the accuracy of the vegetation fraction product used in GLEAM, in this case the Global Vegetation Continuous Fields product (MOD44B). Since the evaporative flux components (i.e., interception loss, soil evaporation and transpiration as well as potential evaporation estimates) are all based on the vegetation fraction cover the accuracy of the vegetation fraction product is a key factor in the overall accuracy (in relation to the Miombo ecosystem) of the estimated evaporation for each land cover. GLEAM is based on four land cover classification that include bare soil, low vegetation (i.e., grass), tall vegetation (i.e., trees), and open water (i.e., lakes). Misclassification of the land cover type will have cascaded effect on several components of the model including the interception loss estimation, multiplicative stress factor which influences the estimation of the various evaporation components in the model.

MOD16 evaporation algorithm is based on the Penman-Monteith equation (Monteith, 1965). The model computes total evaporation as a summation of plant evaporation (canopy interception and transpiration) and soil evaporation utilising both remote sensing and meteorological inputs (Mu *et al*., 2011). MOD16 shows similar patterns with field observations in the green-down and green-up phenophases but gives a slightly different pattern during the dormant phenophase. Field observations, both potential evaporation $E_{c\ (PM)}$ and actual evaporation $E_{a\ (DTS)}$ show the month of June with minimum evaporation. MOD16 shows August as the month with minimum evaporation. This is a two months delay. During the dormant phenophase (i.e., dry season proper) evaporation in the Miombo Forest is through the transpiration process. Possible explanation for this pattern in MOD16 could be attributed to the model structure such as the energy balance module and inputs such as the leaf area index (LAI) and Normalised difference index (NDVI). According to Zimba *et al.* (2020) the lowest long term (2009-2018) MODIS LAI and NDVI monthly minimum and maximum values are observed in August and September respectively and begins to rise in September and October respectively. While MOD16 appear to agree with the vegetation indices LAI and NDVI the start in rise in net radiation in July coupled with long term (2009-2018) NDVI dormant phenophase values of about 0.5 (Zimba *et al*., 2020) which indicate occurrence of health green vegetation with relatively high normalised difference infrared index value (NDII) (indicative of available vegetative moisture state) (Zimba *et al*., 2020) and the already highlighted Miombo species plant water interactions (e.g.., Gumbo *et al*. 2018; Tian *et al*. 2018; Vinya *et al*. 2018**;** Frost 1996) could entail that it is the MOD16 energy balance module which is not well adjusted for the Miombo Woodland. Furthermore, the normalised difference infrared index (NDII), an indicator of plant water status, show negative values or lowest values in August-September (Zimba *et al*., 2020). This might indicate the period when maximum plant water stress is reached. Therefore, the start in increase in net radiation in July is before the plants are highly water stressed and might be the correct start in rise in evaporation as depicted by field observations $E_{a\ (DTS)}$, SSEBop and WaPOR. The underestimation during the dormant and green-up phenophases is probably due to threshold(s) for the canopy/stomata conductance in the transpiration module that might not be correct for the Miombo Woodland for the dormant and green-up phenophases. The key MOD16 component during this period (dormant and start in green-up) is the plant transpiration module driven by land cover/LAI, net radiation, air pressure, air temperature and relative humidity. The link between the highlighted drivers and the assessed plant transpiration is the canopy/stomata conductance thresholds. If the energy balance module and canopy conductance are not appropriately configured for the Miombo Ecosystem this possibly results in the off pattern and underestimation of evaporation during the dormant and green-up phenophases in which evaporation is principally through Miombo Forest transpiration in response to available energy changes. Additionally, daily MOD16 evaporation is a summation of both day and night evaporation. $E_{a\ (DTS)}$ was estimated at hourly scale between 06AM and 06PM which means it does not consider night evaporation. Evaporation values for day time only (about 12 hours) are likely to be different from 24-hour averages for MOD16.

SSEBop is based on the energy balance distinguishing between hot and cold pixels to estimate evaporation. SSEBop actual evaporation is calculated using an evaporation fraction that is based on the hot/dry and cold limiting conditions. To obtain actual evaporation the evaporation fraction is multiplied with the crop coefficient (K_c) and potential evaporation (E_o) (Savoca *et al*., 2013). It appears to have a similar pattern with $E_{a\ (DTS)}$ during the green-down phenophase but slightly differ during the dormant and green-up phenophases in August and December. SSEBop is sensitive to solar radiation/temperature and thus effectively responds to the changes in these variables starting to rise in July as net radiation/temperature begins to rise. The marginal drop in evaporation in August could be attributed to the leaf shedding processes that probably exposes the dry leaf and grass covered

forest floor to more interaction with radiation resulting in increased temperature that is interpreted as non-evaporative surface by SSEBop. Coupled with the relatively (i.e., compared to MOD16 and WaPOR) coarser spatial resolution (i.e., 1 km) the heterogeneity in the leaf fall and leaf flush pattern and the bush fires that normally occur during this period (Gumbo *et al*. 2018; Frost, 1996) could have contributed to this behaviour. SSEBop behaviour in December could be attributed to two factors; cloud cover and the uncertainties associated with estimating land surface temperature (LST) in hot humid conditions (Dash *et al.*, 2002). There is increased cloud cover and rainfall activity in December that affects the quality of the satellite LST product. SSEBop is based on clear sky net radiation balance principle. Zimba *et al*. (2020) indicated that the quality pass for the satellite-based MODIS LST product at the study site was below 80 percent during the rainy season (i.e., December). With reference to $E_{a\ (DTS)}$ the underestimation by SSEBop can be attributed to several factors including the quality of the satellite LST product used and the overpass time of the MODIS satellite over the study site. Like with other products the daily evaporation estimates for SSEBop includes the night time. $E_{a\ (DTS)}$ is estimates are between 6AM and 06 PM. The differences in the time intervals possibly contributes to the observed discrepancy. This is even more important when the 10AM and 1 PM overpass time for MODIS Terra and Aqua which likely affects the minimum and maximum LST estimation consequently affecting the SSEBop actual evaporation estimation.

WaPOR is the only satellite evaporation product with similar pattern with field observation $E_{a\ (DTS)}$ across phenophases and overall (May-December) showed very strong correlation (overall r = 0.80) (Table A4 in the appendices). WaPOR is based on modified Penman-Monteith (P-M) ETLook model which has been adapted to remote sensing inputs (Blatchford *et al*. 2020; FAO, 2018). Actual evaporation is estimated based on seven data components which include precipitation, surface albedo, solar radiation, NDVI, soil moisture stress, land cover and weather data. WaPOR actual evaporation is a summation of interception, soil evaporation and canopy transpiration. WaPOR couples transpiration via the root zone soil moisture content while soil evaporation is coupled via the top soil moisture content. Net radiation is split into soil and canopy net radiation. This implies that increase in LAI exponentially reduces available soil net radiation and increases canopy net radiation. The LAI is derived from the NDVI. WaPOR estimates canopy resistance and establishes the coupled response of soil moisture and LAI on transpiration. The land cover data is used to generate vegetation type dependent stomata conductance thresholds. In WaPOR the classes in the land cover data are used to estimate soil and canopy roughness while the NDVI is used to account for seasonal variations during the growing season (Blatchford *et al.*, 2020). In estimating the soil and canopy aerodynamic resistance WaPOR includes buoyance turbulence using the Monin-Obukhov similarity theory. Therefore, accuracy of land cover product used is likely to influence thresholds for stomata conductance and other land cover type related components of the model. The use of relatively high spatial resolution Copernicus land cover product in WaPOR which has high forest classification accuracy possibly contributes to its ability to capture the vegetation type, which coupled with appropriate parameterisation of the stomata conductance and other vegetation related variables, appear to correctly model the Miombo evaporation pattern. Unlike GLEAM the WaPOR is not a fully net precipitation-based model as it takes into account the vegetation type interaction with the sub-soil moisture content. The soil moisture stress module appears to correctly model the Miombo species behaviour during the three phenophases and most importantly the dormant phenophase which is not properly characterised by other models. Both $E_{a\ (DTS)}$ and WaPOR are dependent on correctly partitioning available energy into sensible and latent heat fluxes. It appears WaPOR energy balance module correctly captures the energy fluxes in the Miombo Forest. The various inputs and processes in the WaPOR, as described above, could go to explain why the model captures the correct evaporation pattern of the Miombo Woodland at the study site. Just like in GLEAM, MOD16 and SSEBop the underestimation by WaPOR can be partly due to the differences in the daily time intervals for the estimation of evaporation as well as the quality of the net radiation product used in the model. WaPOR is estimated over a 24-hour (day) period while $E_{a\ (DTS)}$ was estimated between 06AM and 06 PM.

Generally, the seemingly $E_{a\ (DTS)}$ overestimation, in comparison to satellite products, can be attributed to several factors. Firstly, ground heat flux (G_o) used in the $E_{a\ (DTS)}$ was taken as 10 percent of the diurnal net radiation as per recommendation by Allen *et al.* (1998). It is possible that the G_o was underestimated. Additionally, in this study the biomass storage was not accounted for which potentially made available energy for *H* and *LE* partitioning to be slightly higher than the actual. Furthermore, it is important to note the observation by Schilperoort *et al*. (2018) in which they showed that compared to the EC the DTS method slightly overestimated diurnal *LE* (mean difference of 18.7 $W.m^2$). As shown in Figure 4 it is possible that the relatively warm water from the tank flowing down the cable did not always reach the wet bulb temperature even at 15.5 m height, consequently, the diurnal (especially around peak solar radiation periods) actual vapour pressure could have been overestimated by the DTS measurements leading to relative underestimation of the Bowen ratio and slight overestimation of the latent heat

flux/evaporation. All these factors may have contributed to have slightly higher BR-DTS evaporation estimates than actual field conditions and as compared to the satellite products GLEAM, MOD16, SSEBop and WaPOR. However, using the water balance approach Zimba *et al*. (2022a) showed that satellite products generally underestimate evaporation in the largely Miombo Forest covered Luangwa Basin. The observed pattern in $E_{a\,(DTS)}$ is the correct representation of the Miombo Forest moisture feedback trajectory at the study site. Therefore, the outcome of this study's comparison of point-based observations of Miombo Forest evaporation with satellite evaporation products agree with the larger picture at the Luangwa Basin scale. This is potentially the correct representation of satellite evaporation products behaviour in all Miombo Forest covered basins. However, further studies like this one are needed in the different Miombo ecosystem stratifications in Africa.

4.0 Conclusions and recommendations

The study sought to measure and characterise evaporation in the Miombo Forest across three phenophases at point scale using the BR-DTS approach. To our knowledge this the first independent effort at energy portioning in the Miombo Forest using the BR-DTS approach. Consequently, four satellite evaporation products were compared with the $E_{a\,(DTS)}$. Major conclusions from the study are that:

The BR-DTS approach appear to have correctly captured the moisture feedback of the Miombo Forest across different canopy phenophases. Evaporation patterns appear to be rather influenced by the available energy for evaporation than the characteristic canopy display dynamics during the three phenophases. Across the three canopy phenophases analysed, evaporation follows the net radiation/ air temperature pattern. During the dry season the Miombo species may not be as water stressed as imagined and possibly have developed a dry season water stress buffering mechanism (i.e., access to ground water or vegetative water storage) and transpire within the buffer thresholds. Therefore, coupling the canopy transpiration with the root zone storage, taking into account the vertical upward (beyond 2.5 m) and horizontal moisture flux is likely to improve evaporation assessments in the Miombo Forest.

Compared to $E_{a\,(DTS)}$ all satellite products underestimate evaporation, although this result could have been, to some extent, influenced by the already highlighted potential contributing factors in the preceding section 3.6. It appears that the spatial resolution of satellite products is of influence, as the underestimation is clearly observable with reference to each satellite product's spatial scale i.e., the finer the spatial resolution the lower the underestimation. However, MOD16 and SSEBop with different spatial resolutions (500m and 1000m respectively) appear to have similar results, which may challenge this assumption. What is important to note is that WaPOR is a continental product while the other products are at global scale.

Consequently, of the four satellite products considered in study WaPOR appears to correctly capture the moisture feedback of the Miombo forest across the three canopy phenophases, as it highly correlates with the $E_{a\,(DTS)}$ at the study site. Cumulatively WaPOR also shows the least underestimation. For the wet Miombo Forest, as represented by our study site, and limited to the four models assessed, the WaPOR represents a better choice for use as an evaporation product across the assessed Miombo Forest canopy phenophases. With inference based on WaPOR it appears that modelling evaporation at a scale that takes into account the local variations in the model input variables might give better results

This study was done in the wet Miombo Woodland; therefore, it is possible that the phenological response to changes in available energy and hydrological regimes in the drier Miombo Forest are different from the observations at the Mpika site. There is need for similar observations like this study to be done in the drier Miombo Forest and to compare the results.

Funding

This study was done with the financial support of the Dutch Research Council (NWO) under the project number W 07.303.102.

Author contribution

Conceptualization, H.Z.; formal analysis, H.Z., B.S; resources, H.S.; supervision, M.C.-G. and B.K.; writing—original draft, H.Z.; writing—review and editing, M.C.-G., B.K., H.S., B.S., I.N., and N.V. All authors have read and agree to the published version of the manuscript.

Acknowledgements

The authors wish to thank Nsanzala Conservancy in Mpika, Zambia for hosting the research throughout the study period. We wish to thank the Manager for the valuable contribution in local plant species identification and for

maintaining the study site and equipment. This study would not have been possible without the input of the conservancy.

Data availability: The data used in this study are available online from the 4TU data repository (https://doi.org/10.4121/20492934.v1; Zimba *et al.,* 2022c)

Conflict of interest: Authors declare no conflict of interest

Appendices

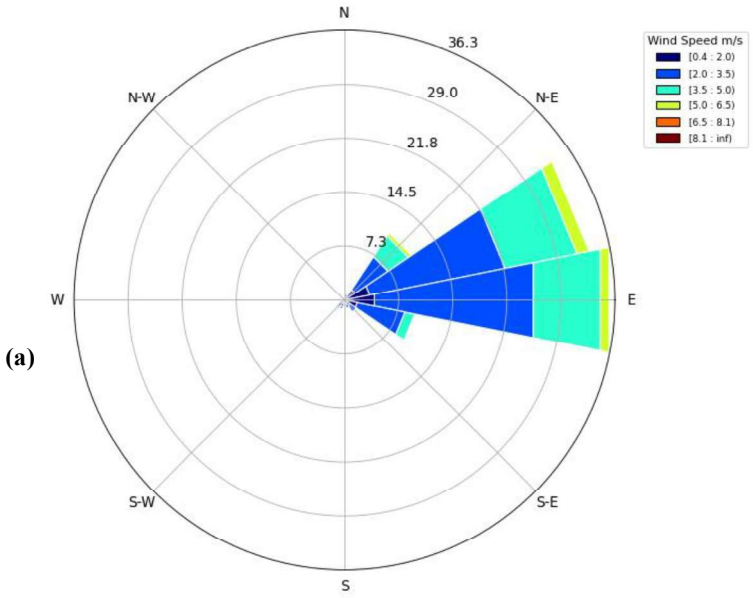

(a)

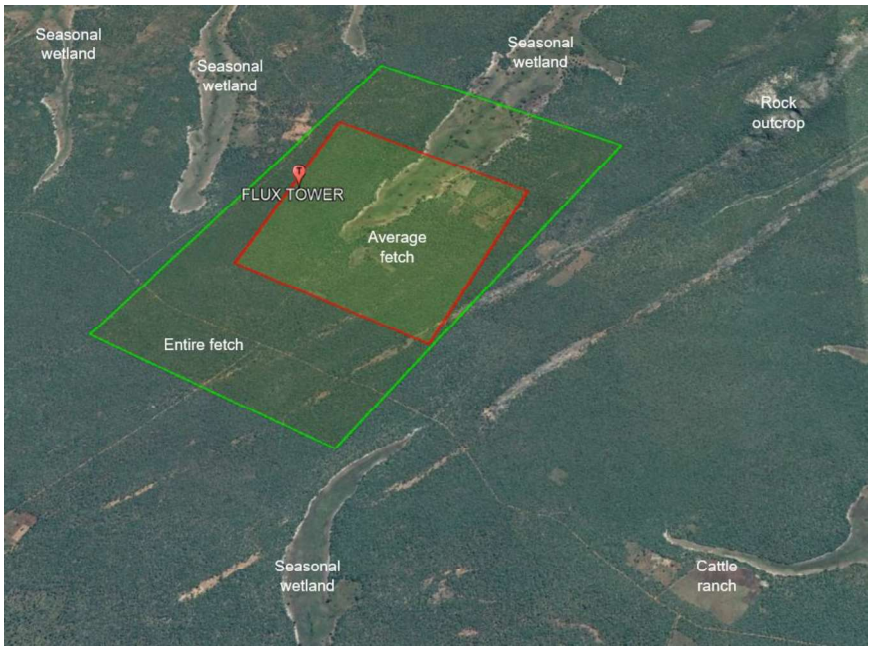

(b)

Figure A1. Analysis of the wind direction and wind speed using the wind rose (a) and the extent of the fetch for the DTS observations (b) based on the wind rose results.

Table A1. Sensing capabilities of the Silixa XT-DTS used in the study

Range	Channels	Resolution			Measurement time	Fiber type	Referencing
		Sampling	Temperature	Spatial			
0 – 10 km	4	25 cm	0.01ºC	60 cm	≥ 5 sec	50/125µm multimode	X2 PT-100 probes

Table A2. Selected ATMOS 41 sensor specifications

Attribute	Air temperature (ºC)	Actual vapour pressure (kPa)	Relative humidity (%)	Wind speed (m/s)	Barometric pressure (kPa)
Range	-50 to 60	0 - 47	0–100% RH (0.00–1.00)	0–30 m/s	50 - 110
Resolution	0.1	0.01	0.1% RH	0.01 m/s	0.01
Accuracy	± 0.6	± 0.2 typical below 40ºC (varies with temperature and humidity)	Varies with temperature and humidity, ±3% RH typical	The greater of 0.3 m/s or 3% of measurement	± 0.1 kPa from -10 to 50 ºC ± 0.5 kPa from -40 to 60 ºC

Table A3. Descriptive statistics of evaporation products at decadal scale

Canopy phenophase	Product	No. of observations	Minimum	Maximum	Median	Sum	Mean	Variance (n-1)	Standard deviation (n-1)	Variation coefficient
Green - Down	$E_{c\ (PM)}$	6	30.86	47.20	39.37	237.86	39.64	37.36	6.11	0.14
	$E_{a\ (DTS)}$	6	14.01	30.17	25.25	146.62	24.44	36.67	6.06	0.23
	GLEAM	6	15.06	27.98	21.96	131.49	21.92	29.74	5.45	0.23
	MOD16	6	24.88	36.83	27.74	176.26	29.38	21.43	4.63	0.14
	SSEBop	6	16.54	25.48	20.89	126.43	21.07	12.74	3.57	0.15
	WaPOR	6	14.70	28.91	24.38	133.17	22.20	33.16	5.76	0.24
Dormant	$E_{c\ (PM)}$	9	37.34	69.46	49.10	471.32	52.37	164.90	12.84	0.23
	$E_{a\ (DTS)}$	9	22.86	51.95	37.10	341.75	37.97	82.85	9.10	0.23
	GLEAM	9	6.55	13.30	9.33	84.69	9.41	4.68	2.16	0.22
	MOD16	9	17.23	24.14	21.23	193.78	21.53	4.07	2.02	0.09
	SSEBop	9	14.78	45.98	25.30	226.79	25.20	100.45	10.02	0.37
	WaPOR	9	15.20	27.15	23.97	204.93	22.77	16.02	4.00	0.17
Green - Up	$E_{c\ (PM)}$	8	56.39	84.11	68.29	558.88	69.86	124.49	11.16	0.15
	$E_{a\ (DTS)}$	8	40.91	77.91	59.09	479.97	60.00	163.14	12.77	0.20
	GLEAM	8	5.40	21.95	11.18	94.25	11.78	34.56	5.88	0.47
	MOD16	8	27.93	53.19	34.72	311.88	38.98	98.20	9.91	0.24
	SSEBop	8	19.61	46.70	36.78	280.25	35.03	96.59	9.83	0.26
	WaPOR	8	33.06	54.52	42.15	338.64	42.33	63.47	7.97	0.18

Table A4. Correlation statistics (Pearson r) of the comparison at decadal scale

Evaporation	$E_{c\ (PM)}$	$E_{a\ (DTS)}$	GLEAM	MOD16	SSEBop	WaPOR
$E_{c\ (PM)}$	**1.00**	**0.95**	**-0.49**	0.37	**0.53**	**0.82**
$E_{a\ (DTS)}$		**1.00**	**-0.53**	**0.47**	**0.53**	**0.84**
GLEAM			**1.00**	0.22	-0.22	-0.15
MOD16				**1.00**	0.06	**0.75**
SSEBop					**1.00**	**0.45**
WaPOR						**1.00**

Values in bold are different from 0 with a significance level alpha=0.05

References

Allen, R. G., Pereira, L. S., Raes, D., & Smith, M.: *FAO Irrigation and Drainage Paper No. 56 - Crop Evapotranspiration*. *56*, 1998.

Angus, D. E., & Watts, P. J.: Evapotranspiration - How good is the Bowen ratio method? *Agricultural Water Management*, *8*(1–3), 133–150. doi: 10.1016/0378-3774(84)90050-7, 1984.

Blatchford, M. L., Mannaerts, C. M., Njuki, S. M., Nouri, H., Zeng, Y., Pelgrum, H., Wonink, S., & Karimi, P.. Evaluation of WaPOR V2 evapotranspiration products across Africa. *Hydrological Processes*, *34*(15), 3200–3221. doi: 10.1002/hyp.13791, 2020.

Bowen, I. S.: The ratio of heat losses by conduction and by evaporation from any water surface. *Physical Review*, *27*(6), 779–787. doi: 10.1103/PhysRev.27.779,1926.

Buttar, N. A., Yongguang, H., Shabbir, A., Lakhiar, I. A., Ullah, I., Ali, A., Aleem, M., & Yasin, M. A.: Estimation of evapotranspiration using Bowen ratio method. *IFAC-PapersOnLine*, *51*(17), 807–810. doi: 10.1016/j.ifacol.2018.08.096,2018.

Chidumayo, E. N.: Climate and Phenology of Savanna Vegetation in Southern Africa. *Journal of Vegetation Science*, *12*(3), 347. doi: 10.2307/3236848, 2001.

Chidumayo, Emmanuel N., & Gumbo, D. J.: The dry forests and woodlands of Africa: Managing for products and services. In The Dry Forests and Woodlands of Africa: Managing for Products and Services (Issue September). doi: 10.4324/9781849776547, 2010.

Cho, J., Oki, T., Yeh, P. J. F., Kim, W., Kanae, S., & Otsuki, K.: On the relationship between the Bowen ratio and the near-surface air temperature. *Theoretical and Applied Climatology*, *108*(1–2), 135–145. doi: 10.1007/s00704-011-0520-y, 2012

Dash, P., Göttsche, F. M., Olesen, F. S., & Fischer, H.: Land surface temperature and emissivity estimation from passive sensor data: Theory and practice-current trends. *International Journal of Remote Sensing*, *23*(13), 2563–2594. doi: 10.1080/01431160110115041,2002.

Euser, T., Luxemburg, W. M. J., Everson, C. S., Mengistu, M. G., Clulow, A. D., & Bastiaanssen, W. G. M.: A new method to measure Bowen ratios using high-resolution vertical dry and wet bulb temperature profiles. *Hydrology and Earth System Sciences*, *18*(6), 2021–2032. doi: 10.5194/hess-18-2021-2014,2014.

FAO.: WaPOR Database Methodology: Level 1 Data. In Remote Sensing for Water Productivity Technical Report: Methodology Series. (Issue September). Retrieved from http://www.fao.org/fileadmin/user_upload/faoweb/RS-WP/pdf_files/Web_WaPOR-beta_Methodology_document_Level1.pdf, 2018.

Foken, T.: THE ENERGY BALANCE CLOSURE PROBLEM: AN OVERVIEW. *Ecological Applications*, *18*(6), 1351–1367. doi: 10.1890/06-0922.1,2008.

Foken, T., Aubinet, M., & Leuning, R.: Eddy Covariance. *Eddy Covariance*. doi: 10.1007/978-94-007-2351-1,2012.

Frost, P.: The Ecology of Miombo Woodlands. In The Miombo in Transition: Woodlands and Welfare in Africa. Retrieved from http://books.google.com/books?hl=nl&lr=&id=rpildJJVdU4C&pgis=1, 1996.

Gumbo, D. J., Dumas-Johansen, M., Muir, G., Boerstler, F., & Xia, Z.: Sustainable management of Miombo woodlands-Food security, nutrition and wood energy. In Food security, nutrition and wood energy. (Issue March). Retrieved from www.fao.org/publications,2018.

Hachigonta, S., & Reason, C. J. C.: Interannual variability in dry and wet spell characteristics over Zambia. *Handbook of Environmental Chemistry, Volume 5: Water Pollution*, *32*(1), 49–62. doi: 10.3354/cr032049, 2006.

Helsel, D. R., Hirsch, R. M., Ryberg, K. R., Archfield, S. A., & Gilroy, E. J.: Statistical Methods in Water Resources Techniques and Methods 4 – A3. *USGS Techniques and Methods*, 2020.

Hunink, J.E. , Terink, W, Contreras, S, D. P.: *Scoping Assessment of Erosion Levels for the Mahale region, Lake Tanganyika, Tanzania* (Vol. 31, Issue August). Retrieved from www.futurewater.nl, 2015.

Martens, B., Miralles, D. G., Lievens, H., Van Der Schalie, R., De Jeu, R. A. M., Fernández-Prieto, D., Beck, H. E., Dorigo, W. A., & Verhoest, N. E. C.: GLEAM v3: Satellite-based land evaporation and root-zone soil moisture. *Geoscientific Model Development*, *10*(5), 1903–1925. doi: 10.5194/gmd-10-1903-2017, 2017.

Meter Group AG.: Atmos 41. In Manual (Issues 207–2022). München. Retrieved from http://library.metergroup.com/Manuals/20635_ATMOS41_Manual_Web.pdf, 2020.

Monteith, J. L.: Evaporation and environment. *Symposia of the Society for Experimental Biology*, *19*, 205, 1965.

Mu, Q., Zhao, M., & Running, S. W.: Improvements to a MODIS global terrestrial evapotranspiration algorithm. *Remote Sensing of Environment*, *115*(8), 1781–1800. doi: 10.1016/j.rse.2011.02.019, 2011.

Olson, D. M., Dinerstein, E., Wikramanayake, E. D., Burgess, N. D., Powell, G. V. N., Underwood, E. C., D'Amico, J. A., Itoua, I., Strand, H. E., Morrison, J. C., Loucks, C. J., Allnutt, T. F., Ricketts, T. H., Kura, Y., Lamoreux, J. F., Wettengel, W. W., Hedao, P., & Kassem, K. R.: Terrestrial ecoregions of the world: A new map of life on Earth. *BioScience*, *51*(11), 933–938. doi: 10.1641/0006-3568(2001)051[0933:TEOTWA]2.0.CO;2, 2001.

Ritter, A., & Muñoz-Carpena, R.. Performance evaluation of hydrological models: Statistical significance for reducing subjectivity in goodness-of-fit assessments. *Journal of Hydrology*, *480*, 33–45. doi: 10.1016/j.jhydrol.2012.12.004, 2013.

Savoca, M. E., Senay, G. B., Maupin, M. A., Kenny, J. F., & Perry, C. A.: Actual Evapotranspiration Modeling Using the Operational Simplified Surface Energy Balance (SSEBop) Approach. *U.S Geologica Survey Scientific Investigations Report 2013–5126*, *January*, 16 p. Retrieved from http://pubs.usgs.gov/sir/2013/5126, 2013.

Schilperoort, B., Coenders-gerrits, M., Luxemburg, W., Rodríguez, C. J., Vaca, C. C., Savenije, H., Rica, T. D. C., Forestal, E. D. I., & Rica, C.: *Technical note : Using distributed temperature sensing for Bowen ratio evaporation measurements*. 819–830, 2018.

Schilperoort, B., Coenders-gerrits, M., Rodríguez, C. J., Tol, C. Van Der, Forestal, E. D. I., Rica, T. D. C., & Rica, C.: *Decoupling of a Douglas fir canopy : a look into the subcanopy with continuous vertical temperature profiles*. 6423–6439, 2020.

Silixa Ltd.: *Silixa XT-DTS Hardware Manual Version 1.3.* Retrieved from www.silixa.com, 2016.

Spittlehouse, D. L., & Black, T. A.: Evaluation of the bowen ratio/energy balance method for determining forest evapotranspiration. *Atmosphere - Ocean*, *18*(2), 98–116. doi: 10.1080/07055900.1980.9649081, 1980.

Sriwongsitanon, N., Gao, H., Savenije, H. H. G., Maekan, E., Saengsawang, S., & Thianpopirug, :S. The Normalized Difference Infrared Index (NDII) as a proxy for soil moisture storage in hydrological modelling. *Hydrology and Earth System Sciences Discussions*, *12*(8), 8419–8457. doi: 10.5194/hessd-12-8419-2015, 2015.

Sutanto, S. J., Wenninger, J., & Uhlenbrook, S.: Partitioning of evaporation into transpiration, soil evaporation and interception: a combination of hydrometric measurements and stable isotope analyses. *Hydrology and Earth System Sciences Discussions*, *9*(3), 3657–3690. doi: 10.5194/hessd-9-3657-2012, 2012.

Teuling, A. J.: A Forest Evapotranspiration Paradox Investigated Using Lysimeter Data. *Vadose Zone Journal*, *17*(1), 170031. doi: 10.2136/vzj2017.01.0031, 2018.

Tian, F., Wigneron, J. P., Ciais, P., Chave, J., Ogée, J., Peñuelas, J., Ræbild, A., Domec, J. C., Tong, X., Brandt, M., Mialon, A., Rodriguez-Fernandez, N., Tagesson, T., Al-Yaari, A., Kerr, Y., Chen, C., Myneni, R. B., Zhang, W., Ardö, J., & Fensholt, R.: Coupling of ecosystem-scale plant water storage and leaf phenology observed by satellite. *Nature Ecology and Evolution*, *2*(9), 1428–1435. doi: 10.1038/s41559-018-0630-3, 2018.

van de Giesen, N., Steele-Dunne, S. C., Jansen, J., Hoes, O., Hausner, M. B., Tyler, S., & Selker, J.: Double-ended calibration of fiber-optic raman spectra distributed temperature sensing data. *Sensors (Switzerland)*, *12*(5), 5471–5485. doi: 10.3390/s120505471, 2012.

Van Der Ent, R. J., Wang-Erlandsson, L., Keys, P. W., & Savenije, H. H. G.: Contrasting roles of interception and transpiration in the hydrological cycle – Part 2: Moisture recycling. *Earth System Dynamics*, *5*(2), 471–489. doi: 10.5194/esd-5-471-2014, 2014.

Vinya, R., Malhi, Y., Brown, N. D., Fisher, J. B., Brodribb, T., & Aragão, L. E. O. C.: *Seasonal changes in plant – water relations in fl uence patterns of leaf display in Miombo woodlands : evidence of water conservative strategies*. *Fuller 1999*, 104–112. doi: 10.1093/treephys/tpy062, 2018.

White, F.: *The vegetation of Africa*. Paris: UNESCO, 1984.

Xing, Zisheng, Lien Chow, Fan-Rui Meng, Herb W. Rees, Lionel Steve, and J. M.: Validating Evapotranspiraiton Equations Using Bowen Ratio in New Brunswick, Maritime, Canada. *Sensors*, *1*, 412-428. Retrieved from https://doi.org/10.3390/s8010412, 2008.

Zimba, H, Coenders-Gerrits, M., Banda, K., Hulsman, P., van de Giesen, N., Nyambe, I., & Savenije, H.: On the importance of phenology in the Miombo ecosystem: Evaluation of open-source satellite evaporation models. *Hydrol. Earth Syst. Sci. Discuss.*, *2022*(April), 1–42. Retrieved from https://hess.copernicus.org/preprints/hess-2022-114/%0Ahttps://hess.copernicus.org/preprints/hess-2022-114/hess-2022-114.pdf, 2022a.

Zimba, Henry; Coenders, Miriam; Schilperoort, Bart; Savenije, Hubert H.G.; van de Giesen, N. *ZAMSECUR Project Field Data Mpika, Zambia.* 4TU.ResearchData. doi: https://doi.org/10.4121/19372352.v2, 2022b.

Zimba, Henry; Savenije, Hubert H.G.; van de Giesen, Nick; Coenders, Miriam; Schilperoort, Bart. ZAMSECUR Project Miombo Forest, Zambia, Southern Africa. 4TU.ResearchData. Dataset. https://doi.org/10.4121/20492934.v1, 2022c.

Zimba, Henry, Coenders-Gerrits, M., Kawawa, B., Savenije, H., Nyambe, I., & Winsemius, H.: Variations in canopy cover and its relationship with canopy water and temperature in the miombo woodland based on satellite data. *Hydrology*, *7*(3). doi: 10.3390/HYDROLOGY7030058, 2020.